Learning from Directed Evolution: Theoretical Investigations into Cooperative Mutations in Lipase Enantioselectivity

Marco Bocola,[a] Nikolaj Otte,[a] Karl-Erich Jaeger,[b] Manfred T. Reetz,[a] and Walter Thiel*[a]

Molecular modeling with classical force-fields has been used to study the reactant complex and the tetrahedral intermediate in lipase-catalyzed ester hydrolysis in 20 enzyme/substrate combinations. The R *and* S *enantiomers of* α*-methyldecanoic acid ester served as substrates for the wild-type lipase from* Pseudomonas aeruginosa *and nine selected mutants. After suitable preparation of initial structures from an available wild-type crystal structure, each system was subjected to 1 ns CHARMM force-field molecular dynamics simulations. The resulting geometric and energetic changes allow interpretation of some experimentally observed effects of mutations, particularly with regard to the "hot spots" at residues 155 and 162. The replacement S155F enhances* S *enantiopreference through a steric relay involving Leu162. The double mutation S53P + L162G improves* S *enantioselectivity by creating a new binding pocket for the* S *enantiomer with an additional stabilizing hydrogen bond to His83. The simulations provide insight into remote and cooperative effects of mutations.*

Introduction

We have previously demonstrated that the methods of directed evolution[1–3] can be applied successfully in the quest to create enantioselective enzymes for use in synthetic organic chemistry.[4, 5] The underlying concept involves repeating cycles of random gene mutagenesis and expression, coupled with high-throughput screening for enantioselectivity,[6] a "Darwinian" process that goes beyond simple combinatorial catalysis. The "inferior" enzymes and genes are discarded, and the genetic information in the best gene encoding the most enantioselective enzyme is passed onto the next generation, a strategy that does not require any knowledge of the structure or mechanism of the enzyme. It is thus quite different from other forms of protein engineering in which rational design based on molecular modeling is used as a guide for performing site-specific mutagenesis at predetermined positions in the enzyme.[7] Nevertheless, structural and mechanistic lessons can be learned after optimization of a given catalytic property by directed evolution.[1–5] Arnold, for example, has exploited the methods of directed evolution in order to convert subtilisin E into a functional equivalent of thermitase, sequence analysis of the thermally most stable mutant showing amino acid substitutions almost exclusively at positions far away from the active site.[8] Such remote effects, which would be unlikely to be discovered by "rational protein engineering", were linked to the improvement of hydrogen bonding near a β-bulge and to reduced cavity volume. Several other cases of remote effects on enzyme properties have also been reported.[9]

In our original study we used repeating error-prone polymerase chain reaction (epPCR) cycles to increase the enantioselectivity of the kinetic resolution of *rac*-2-methyldecanoic acid *p*-nitrophenol ester (**1**) catalyzed by the lipase from *Pseudomonas aeruginosa*.[4] The wild-type leads to a selectivity factor of only $E = 1.1$ (Scheme 1).

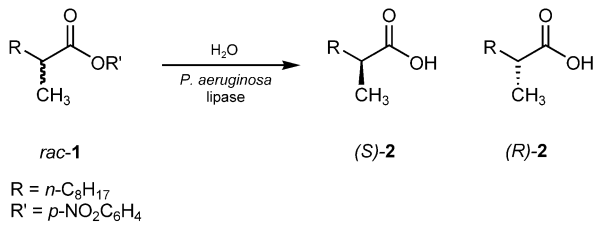

Scheme 1. *Kinetic resolution of rac-2-methyldecanoic acid* p*-nitrophenol ester (**1**) catalyzed by the lipase from* Pseudomonas aeruginosa.

After just four epPCR cycles at low mutation rate, an enzyme mutant showing markedly enhanced enantioselectivity ($E = 11.3$) was identified.[4a] In further optimization studies, saturation

[a] *Dr. M. Bocola, N. Otte, Prof. M. T. Reetz, Prof. W. Thiel*
Max-Planck-Institut für Kohlenforschung
Kaiser-Wilhelm-Platz 1
45470 Mülheim an der Ruhr (Germany)
Fax: (+49) 208-306-2996
E-mail: thiel@mpi-muelheim.mpg.de

[b] *Prof. K.-E. Jaeger*
Institut für Molekulare Enzymtechnologie
Heinrich-Heine-Universität Düsseldorf
Forschungszentrum Jülich
52426 Jülich (Germany)

  DOI: 10.1002/cbic.200300731

mutagenesis at selected "hot spots" corresponding to the mutations identified by sequence analysis, followed by additional epPCR, led to an even better mutant displaying an *E* value of 25.8.[4b] This mutant is characterized by five mutational changes, all of which occur at remote positions. Although no crystal structures of the mutant lipases from *Pseudomonas aeruginosa* are yet available, the X-ray structure of the wild-type is known.[10a] In our work the observation of remote effects came as a surprise, since stereoselectivity is traditionally associated with geometric complementarity at the active site. Indeed, all "rational" attempts to improve the enantioselectivity of enzymes have focused on site-specific mutagenesis near the active site,[7] in accord with Emil Fischer's lock-and-key hypothesis or refined models.[11] In our case, simple molecular modeling led to the preliminary conclusion that increased flexibility may be responsible for enhanced enantioselectivity.[4b]

After these early studies,[4a,b] we continued to explore protein sequence space by applying a special form of DNA shuffling:[2] combinatorial cassette mutagenesis (CMCM).[4c] This culminated in the identification of the currently most enantioselective mutant 1H8 ($E > 51$), with six mutational changes. This is not only the most enantioselective variant, but is also considerably more active than the wild-type. On going from the wild-type to 1H8, the k_{cat}/K_m value increases significantly: for *(S)*-**1**, $k_{cat}/K_m = 9.0 \times 10^2\,M^{-1}s^{-1}$ (wild-type) and $3.7 \times 10^5\,M^{-1}s^{-1}$ (variant 1H8), and for *(R)*-**1**, $k_{cat}/K_m = 3.5 \times 10^2\,M^{-1}s^{-1}$ (wild-type) and $8.4 \times 10^3\,M^{-1}s^{-1}$ (variant 1H8).[5d]

Understanding the enhanced enantioselectivity achieved by directed evolution[4, 5, 9e, 12] is a major challenge. This study marks the first phase of a theoretical investigation directed toward this goal. It addresses lipase enantioselectivity in the wild-type and in several mutants including 1H8. Here we describe the results from extensive molecular mechanical (MM) modeling for reactive intermediates. Quantum mechanical (QM) calculations of transition states in the context of QM/MM approaches will be reported at a later stage.

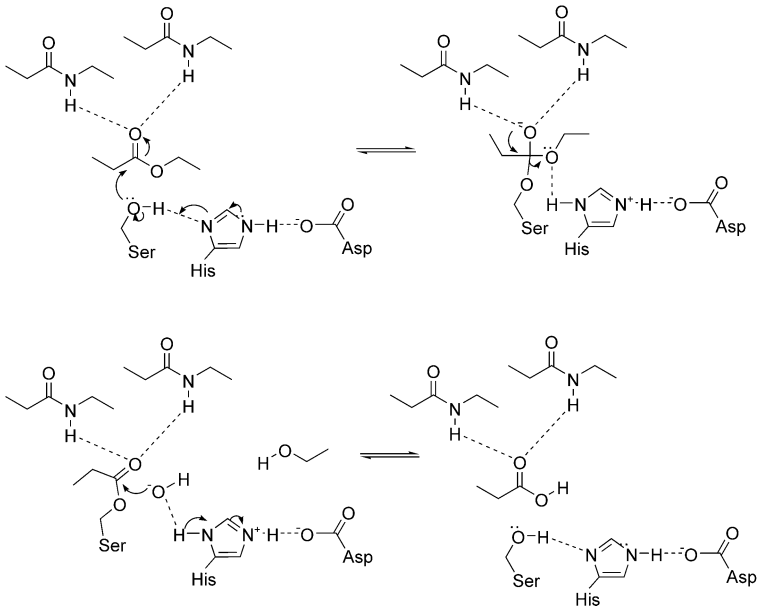

Scheme 2. *Mechanism of lipase-catalyzed ester hydrolysis.*

Results and Discussion

Structural and mechanistic background

This theoretical study is based on information provided by X-ray structural analysis[10] of the lipase from *Pseudomonas aeruginosa* (wild-type). It shows a conserved α/β hydrolase fold typical of lipases (EC 3.1.1.3)[13] and the presence of the usual catalytic triad composed of aspartate (D229), histidine (H251), and serine (S82). Compared to the I.2 family of lipases,[13] the C-terminal antiparallel β sheet is missing, revealing more compact packing of the molecule. The usual helical lid is present. The mechanism of ester hydrolysis catalyzed by this enzyme is typical of lipases (see Scheme 2). After formation of the noncovalently bound Michaelis – Menten reactant complex between the ester and the enzyme, a proton shuttle activates serine, which then adds nucleophilically to the ester function to yield a tetrahedral intermediate (TI), which is stabilized by hydrogen bonding to nearby backbone amide groups. Donation of a proton from the histidine residue liberates the corresponding alcohol and generates a covalently bound acyl-enzyme intermediate, which reacts with water to form the product complex between the acid and the enzyme. The final step in the catalytic process is the release of the acid.

A schematic energy profile for this mechanism is shown in Figure 1. It is commonly accepted that the transition states leading to the tetrahedral intermediate are rate-determining,

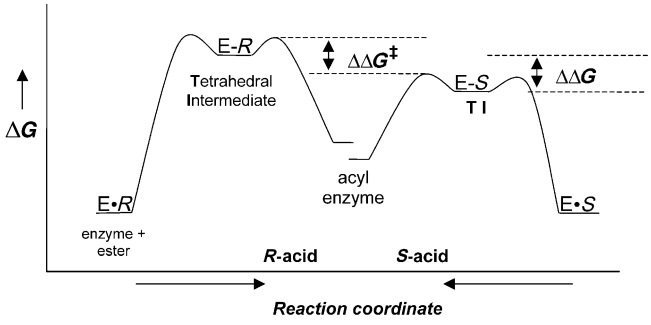

Figure 1. *Schematic energy profile for the conversion of the Michaelis – Menten complex to the acyl enzyme via the tetrahedral intermediate. We assume that the energy difference $\Delta_{R\text{-}S}\Delta G$ for the two tetrahedral intermediates closely resembles the rate-determining energy difference $\Delta_{R\text{-}S}\Delta G^{\ddagger}$ between the transition states for both enantiomers.*

and so the modeling of enantioselectivity should focus on these transition states and evaluate the difference $\Delta_{R\text{-}S}\Delta G^{\ddagger}$ in the free energy barriers for *R* and *S* substrates. We have studied the relevant minima and transition states in a model system (Scheme 3) through quantum-chemical calculations by different

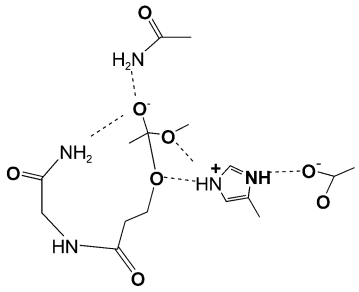

Scheme 3. *Model system for quantum-chemical studies of the lipase mechanism. The model contains the essential side-chain atoms of the catalytic triad Asp, His, and Ser. The oxy-anion hole is modeled by an isolated acetamide and the backbone atoms of Ser and of the adjacent residue, which forms part of the oxy-anion hole according to the lipase crystal structure.[10] The negatively charged tetrahedral intermediate is represented by a methylacetate covalently bound to the SerOγ atom. Dotted lines indicate H bonds.*

QM methods up to density functional theory at the BLYP/6-31G* level.[14] The optimized transition structures closely resemble the geometries of the corresponding tetrahedral intermediates, as has already been found in other quantum-chemical model studies.[15] The tetrahedral intermediates can thus be regarded as transition state analogues, which suggests that their relative stability $\Delta_{R\text{-}S}\Delta G$ should be a key factor in determining the enantioselectivity of lipase-catalyzed ester hydrolysis (see Figure 1). In analogy with previous modeling studies on lipase enantioselectivity toward triacylglycerols and chiral alcohols,[16] we therefore decided to concentrate on the tetrahedral intermediates in our initial MM explorations of ester hydrolysis with different lipase mutants. In addition, we have also investigated the noncovalently bound Michaelis – Menten complex to see whether there is any enantiodiscrimination in the first step of the reaction.

Choice of mutants

Figure 2 shows the crystal structure of the wild-type lipase from *Pseudomonas aeruginosa* with a covalently bound phosphonate inhibitor.[10a] The most enantioselective mutant (1H8) found so far in our studies on directed evolution (see above) has six mutations, marked in yellow: namely, D20N, S53P, S155M, L162G, T180I, and T234S. Only one of these mutations (L162G) is located directly at the active site near the substrate. The residues involved in the two next-nearest mutations (S53P, S155M) are already more than 10 Å away from the active site, the latter (S155M) involving a serine residue that accounts for the only hydrogen bond to the lid helix at position N132 (see Figure 3). The three most distant mutations (D20N, T180I, T234S) are located at the surface of the enzyme very far away from the active site (more than 13 Å).

To understand the source of lipase enantioselectivity, we have studied not only the wild-type enzyme and the best mutant 1H8, but also eight other mutants to check for the influence of single mutations and for cooperative effects. Obvious candidates are the single mutants of the wild-type enzyme, which contain just one of the replacements observed in the 1H8 mutant. We

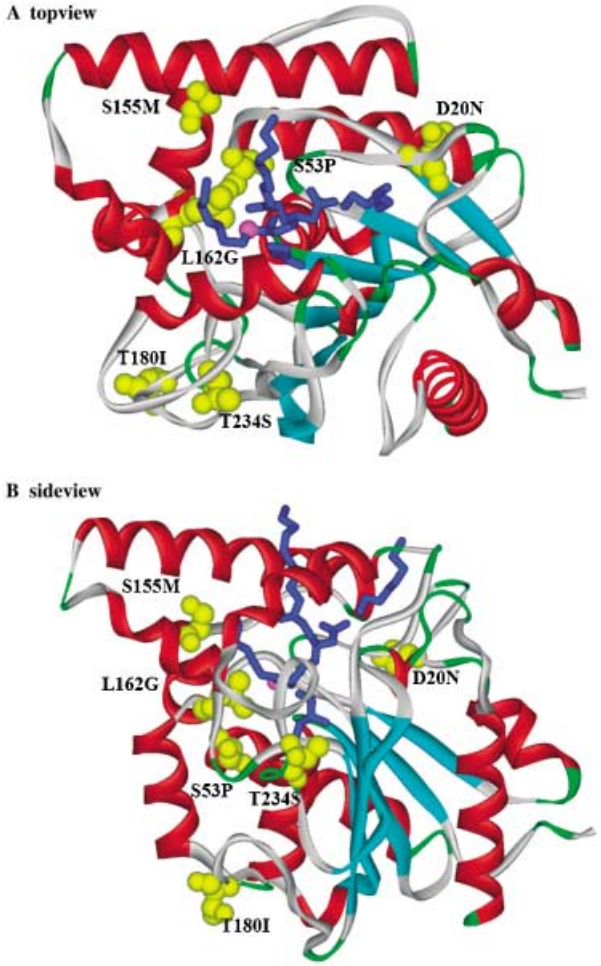

Figure 2. *Cartoon of* P. aeruginosa *lipase X-ray crystal structure.[10a] The positions of the six mutations are drawn as van der Waals representations in yellow. The bound phosphonate is shown as a stick representation in blue, the first atom of the bound phosphonate acid moiety (C4) being highlighted in magenta. Only one mutation (L162G) is located directly in the active site near the substrate acid. The exchange S155M is located behind the oxy-anion hole under the lid helix. The mutation S53P also lies behind the oxy-anion hole, but more than 10 Å away from the substrate (C4). Three positions (D20N, T180I, T234S) are located at the surface of the enzyme far away from the active site.*

selected the closest three of these (L162G, S53P, and S155M), and disregarded the distant surface mutations. By the same qualitative reasoning, we also investigated the most promising double (L162G + S53P) and triple (L162G + S53P + S155M) mutants.

Our previous experimental work had shown that residues 155 and 162 are "hot spots" for directed evolution. The exchange L162G has indeed been found most often in successful mutants.[4] On the other hand, the exchange S155M (as in 1H8) has not been encountered in other highly stereoselective mutants, whereas the mutation S155F has often led to large improvements. We therefore also decided to consider three corresponding mutants, with one (S155F), two (L162G + S155F), and three (L162G + S53P + S155F) replacements. The last of these differs from the other triple mutant only at residue 155 (S155F instead of S155M).

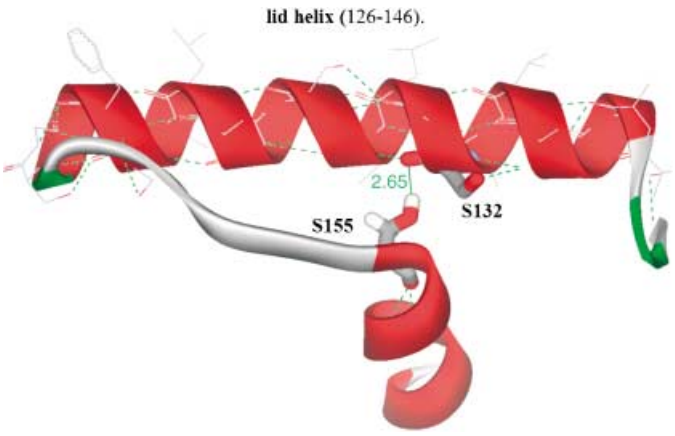

Figure 3. *X-ray crystal structure of* P. aeruginosa *lipase:[10a] Serine155 (shown in stick representation) forms a 2.6 Å long H bond (solid line) with the backbone carbonyl group of Serine132 (shown in stick representation) of the lid helix. This is the only H bond between the lid helix and the rest of the enzyme. The other detected H bonds (dashed lines) are between residues within this helix.*

Of the nine selected mutants, only four have so far been created in directed evolution processes (S155F, L162G, S155F + L162G, 1H8).[4] The other five mutants are included here for computational analysis.

Molecular dynamics (MD) simulations

We have studied complexes derived from (*R*)- and (*S*)-α-methyldecanoic acid (MDA) ester and the lipase from *P. aeruginosa* (wild-type and nine mutants; see above). The initial structures for the MD simulations were prepared from the X-ray structure of the wild-type with a phosphonate inhibitor,[10a] which involved the replacement of this inhibitor by the MDA ester to build the Michaelis – Menten complex or the tetrahedral intermediate, respectively, and the exchange of the relevant residues in the case of the mutants (see above). After assignment of the appropriate protonation state, the systems were relaxed through a series of minimizations and were then subjected to 1 ns MD simulations (300 ps equilibration, 700 ps production runs). The applied procedures are fully specified in the section on computational methods.

Initial studies on the wild-type enzyme and the mutants employed the MAB force-field[17a] with implicit solvation as implemented in the MOLOC software.[17b] The MAB force-field is parameterized to reproduce the free energy of hydration for polar and apolar compounds.[17b] Subsequently, more systematic investigations were performed by use of the CHARMM22/27 force-field[18a–d] with explicit TIP3P solvation for the active site and the CHARMM software[18e] (version 28b2 and 29b2). The results obtained from the MD simulations with these two force-fields were qualitatively similar in all cases studied. For the sake of brevity, we only report the CHARMM results in the following sections. It should be stressed at the outset that the standard deviations of the average results from the MD simulations are generally quite large and that we shall therefore focus on qualitative conclusions rather than on quantitative assessments.

Geometries

Table 1 compares the X-ray geometry of the wild-type enzyme containing a phosphonate inhibitor[10a] with the CHARMM structures of the wild-type and of the mutant 1H8 containing the MDA ester tetrahedral intermediate. It lists the distances between the first carbon atom of the acid moiety in the active site (C4 in the phosphonate[10a] or stereocenter *C1 in MDA, respectively) and the residues involved in the 1H8 mutations (C_α and terminal side-chain atoms). Because of the presence of different substrates, these distances are not directly comparable, but it is still important to note that their overall pattern for the wild-type is the same in the X-ray and in the CHARMM structure, indicating that the overall fold of the enzyme remains conserved during the MD simulations. Likewise, the orientations of the side chains of the six residues considered are the same in both structures, as can be seen from the differences between the distances given for the C_α and the terminal side-chain atoms: the side chains of residues 53 and 162 point toward the active site, while those of the other residues point away from the active site.

Table 1. *Distance of the mutated residues to the acid[a] in the X-ray crystal structure of the wild-type or the 1 ns CHARMM model[b] of the (S)-MDA ester-TI in the wild-type and the mutant 1H8.*

P. ae. lipase mutation	*wild-type (phosphonate) X-ray distance* C_α—*C4*	*distance* X_{term}—*C4*	*wild-type (MDA) CHARMM av. distance* C_α—**C1*	*av. distance* X_{term}—**C1*	*1H8 (MDA) CHARMM av. distance* C_α—**C1*	*av. distance* X_{term}—**C1*
D20N	15.8	17.6	17.3 ± 0.2	18.2 ± 0.3	16.8 ± 0.2	19.0 ± 0.3
S53P	10.9	9.4	10.3 ± 0.2	9.1 ± 0.3	9.7 ± 0.2	8.4 ± 0.6
S155M	11.3	12.6	11.9 ± 0.3	13.6 ± 0.3	11.2 ± 0.2	9.8 ± 0.4
L162G	6.5	4.0	7.6 ± 0.3	4.6 ± 0.8	6.7 ± 0.3	no side chain
T180I	21.8	23.8	21.0 ± 0.2	23.0 ± 0.2	19.9 ± 0.4	22.4 ± 0.4
T234S	13.2	15.2	13.9 ± 0.2	15.8 ± 0.2	12.7 ± 0.2	14.5 ± 0.4

[a] Distance in Å between the first carbon atom in the acid moiety of the bound phosphonate (C4) or the substrate stereocenter (*C1) of the chiral acid and the main-chain C_α atom or the terminal side-chain heavy atom (X_{term}), respectively, of the residue involved in the given mutation. [b] The last 700 ps of 1 ns CHARMM MD simulations were evaluated (see Computational Methods). Average values and corresponding standard deviations were determined for each MD run (350 data points). The mean values from two independent MD runs are given in the table.

On comparing the CHARMM average structures for the wild-type and for the mutant 1H8 (Table 1) we again find a similar pattern for the C_α–*C1 distances (which are generally smaller in 1H8), and the side chains of the surface residues 20, 180, and 234 again point outwards. On the other hand, the side chain of residue 155 adopts a different orientation in the mutant than in the wild-type, now pointing toward the active site (like residue 53). This observation calls for a more careful analysis of the geometric changes in the mutants and their possible effects on enantioselectivity.

Tables 2 and 3 list average values for selected distances in the studied Michaelis–Menten complexes and tetrahedral intermediates, respectively. The chosen distances are defined in Scheme 4. Data are given for the wild-type enzyme and all nine mutants, each in combination with both the *R* and the *S* substrates.

Generally speaking, the variations in the computed average distances for different mutants are smaller for the Michaelis–Menten complexes than for the tetrahedral intermediates. The "nucleophilic" distance *d1* between SerO82γ and the substrate carbonyl carbon atom is fairly uniform in different mutants and is usually slightly smaller for the *S* substrate than for the *R* form (Table 2). The distance *d3*, reflecting the orientation of residue 155 (see above), decreases significantly in relation to the wild-type whenever there is a mutation (S155M, S155F) that disrupts the hydrogen bond to the lid. The reorientation of this residue found in the tetrahedral intermediate of 1H8 (Table 1) is thus a general phenomenon that already occurs in the Michaelis–Menten complex.

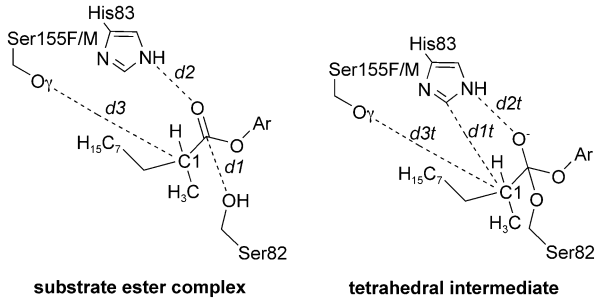

Scheme 4. *Schematic representation of the distance descriptors used in Tables 2 and 3.*

Turning to the tetrahedral intermediates (Table 3), the single mutants S53P and L162G seem to be fairly similar to the wild-type with regard to the chosen geometric descriptors, whereas the single mutants S155M and S155F show the now familiar reorientation of residue 155 due to the lack of ability of methionine and phenylalanine to form a hydrogen bond to the lid helix. In the case of S155F, the average distance *d3t* between the terminal atom of this residue and the stereocenter *C1 decreases from 12.6 Å (wild-type) to 10.0 Å (S155F) for the rapidly reacting *(S)*-MDA ester tetrahedral intermediate, while exhibiting a much smaller reduction from 13.4 to 13.0 Å in the

Table 2. *Geometric descriptors[a] in the (R)- and (S)- MDA ester complexes for the wild-type enzyme and different mutants.[b]*

		wild-type	1H8	S53P S155M L162G	S53P S155F L162G	S53P L162G	S155F L162G	S53P	S155M	S155F	L162G
distance *d1*											
Ser82Oγ-$C_{carbonyl}$	*S*	3.34 ± 0.3	3.29 ± 0.3	3.18 ± 0.2	3.43 ± 0.2	3.32 ± 0.4	3.14 ± 0.2	3.56 ± 0.5	3.18 ± 0.2	3.24 ± 0.2	3.21 ± 0.2
Ser82Oγ-$C_{carbonyl}$	*R*	3.30 ± 0.3	3.68 ± 0.3	3.38 ± 0.3	4.33 ± 0.3	3.83 ± 0.4	3.77 ± 0.3	3.69 ± 0.5	3.65 ± 0.3	3.61 ± 0.4	3.15 ± 0.2
distance *d2*											
His83 Nδ1-oxy	*S*	4.90 ± 0.3	3.83 ± 0.3	4.89 ± 0.3	4.61 ± 0.3	4.72 ± 1.0	5.64 ± 0.3	5.33 ± 0.4	4.68 ± .03	5.37 ± 0.3	4.82 ± 0.3
His83 Nδ1-oxy	*R*	5.84 ± 0.4	5.02 ± 0.3	5.51 ± 0.3	5.61 ± 0.3	4.48 ± 1.0	4.97 ± 0.4	5.36 ± 0.4	5.46 ± 0.3	5.93 ± 0.4	5.38 ± 0.4
distance *d3*											
residue 155 X_{term}-C1	*S*	12.36 ± 0.4	8.41 ± 1.5	8.45 ± 0.5	9.35 ± 0.5	12.80 ± 0.3	9.17 ± 0.4	12.54 ± 0.5	9.80 ± 0.6	9.46 ± 0.6	12.67 ± 0.4
residue 155 X_{term}-C1	*R*	12.74 ± 0.5	8.80 ± 0.5	8.93 ± 0.6	9.69 ± 0.6	12.32 ± 0.4	10.15 ± 0.6	12.87 ± 0.4	9.51 ± 0.5	9.33 ± 0.6	13.41 ± 0.5

[a] Average distances [Å] between the atoms shown in Scheme 4. [b] See footnote [b] of Table 1.

Table 3. *Geometric descriptors[a] in the (R)- and (S)-MDA ester TI for the wild-type enzyme and different mutants.[b]*

		wild-type	1H8	S53P S155M L162G	S53P S155F L162G	S53P L162G	S155F L162G	S53P	S155M	S155F	L162G
distance *d1t*											
His83 Cε-C1	*S*	7.30 ± 0.3	5.29 ± 0.2	4.43 ± 0.3	4.88 ± 0.4	4.03 ± 0.2	4.43 ± 0.2	6.95 ± 0.3	6.89 ± 0.3	6.89 ± 0.2	6.77 ± 0.3
His83 Cε-C1	*R*	8.00 ± 0.2	6.95 ± 0.3	6.88 ± 0.4	6.64 ± 0.2	6.95 ± 0.4	7.00 ± 0.20	7.94 ± 0.2	7.55 ± 0.2	7.40 ± 0.2	6.91 ± 0.3
distance *d2t*											
His83 Nδ1-oxy	*S*	5.13 ± 0.3	2.71 ± 0.2	2.71 ± 0.2	4.01 ± 0.5	2.82 ± 0.2	3.77 ± 0.9	4.88 ± 0.2	5.02 ± 0.2	5.01 ± 0.2	5.41 ± 0.3
His83 Nδ1-oxy	*R*	5.14 ± 0.2	5.15 ± 0.3	5.39 ± 0.4	5.30 ± 0.2	5.32 ± 0.4	5.78 ± 0.2	5.05 ± 0.2	5.45 ± 0.2	5.36 ± 0.2	5.53 ± 0.3
distance *d3t*											
residue 155 X_{term}-C1	*S*	12.60 ± 0.3	9.81 ± 0.6	8.80 ± 0.5	9.12 ± 0.5	12.70 ± 0.3	9.92 ± 0.4	13.00 ± 0.3	9.42 ± 0.5	9.99 ± 0.4	13.36 ± 0.5
residue 155 X_{term}-C1	*R*	13.42 ± 0.3	9.71 ± 0.4	9.22 ± 0.5	9.46 ± 0.5	12.89 ± 0.4	9.41 ± 0.4	13.60 ± 0.3	13.25 ± 0.4	13.04 ± 0.5	12.64 ± 0.4

[a] Average distances [Å] between the atoms shown in Scheme 4. [b] See footnote [b] of Table 1.

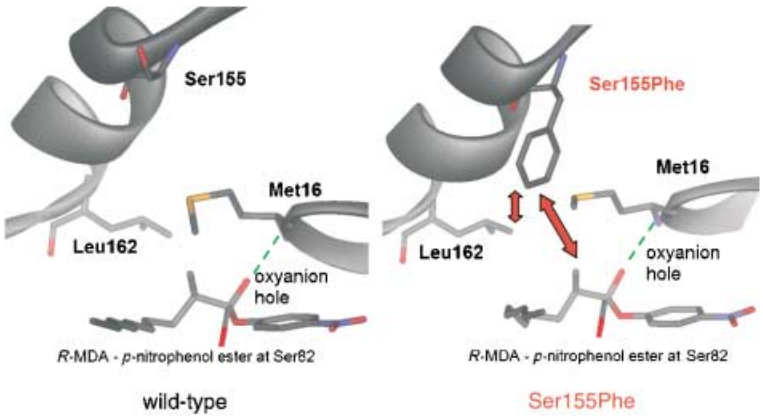

Figure 4. *Relative orientations of the side chain of residue 155 in the wild-type (left) and in the mutant S155F (right): the side chain is oriented toward the lid helix in the wild-type, but toward Leu162 and the active site in the mutant S155F. The slowly reacting (R)-MDA ester TI enantiomer points its α-methyl group (indicated by an asterisk) directly toward Leu162 in all binding modes investigated, suggesting that the moderately selective S155F may act by a steric relay through Leu162. Hydrogen bonds toward Met16 in the oxy-anion hole are indicated by dashed green lines.*

case of the *R* enantiomer. Figure 4 illustrates the steric situation in the wild-type and in the mutant S155F in more detail. The slowly reacting *R* enantiomer points its methyl group directly toward Leu162 in all binding modes investigated, due to the need to orient the long acid chain in the narrow acid pocket, the phenol moiety in the alcohol pocket, and the carbonyl oxygen in the oxy-anion hole. The introduction of a bulky side chain in S155F thus causes considerable steric strain around Leu162 in the *R* enantiomer (Figure 4). On the other hand, the *S* enantiomer, with the methyl group on the opposite side, does not encounter such steric hindrance in S155F and so can relax geometrically (see above). These steric effects favor the *S* enantiomer and should lead to an enhanced enantioselectivity. This argument assumes implicitly that the loss of the hydrogen bond to the lid in S155F does not cause adverse effects due to lid motions that might become possible on time scales longer than our 1 ns simulation.

In the previous experimental work on directed evolution,[4] residue 155 had been identified as a "hot spot". The current MD simulations suggest a mechanism as to how mutations such as S155M and S155F may act in general: the reorientation of the corresponding remote side chain brings it into direct contact with the active site residue Leu162, which is in van der Waals contact with the stereocenter. This steric relay then leads to discrimination between the *S* and *R* enantiomers of the corresponding tetrahedral intermediates (and also of the corresponding transition states, according to our basic assumptions).

The double mutant S53P + L162G resembles the wild-type enzyme with regard to the position of Ser155 (no mutation) but the nonmutated His83 located between residues 53 and 162 may exhibit strong displacements (Table 3). For example, the average distance *d2t* between the histidine Nδ and the oxy-anion atom drops from 5.1 Å in the wild-type to 2.8 Å in the double mutant for the *S* enantiomer, whereas it remains almost unchanged for the *R* enantiomer (5.1 vs. 5.3 Å). Closer inspection shows that an additional hydrogen bond is formed in the sterically unencumbered case of the *S* enantiomer, but not in the *R* enantiomer, where the methyl group at the stereocenter prevents a closer approach between His83 and the negatively charged oxygen atom of the oxy-anion. Figure 5 further illustrates these geometric changes. The replacement L162G removes an isobutyl side chain close to the active center and thus opens up a new binding pocket capable of accommodating α-branched acids directly adjacent to the stereocenter. The slowly reacting *R* enantiomer points its methyl group into this new binding pocket, unlike the rapidly reacting *S* enantiomer, which has its methyl group on the opposite side. In the latter case, the binding pocket can be used

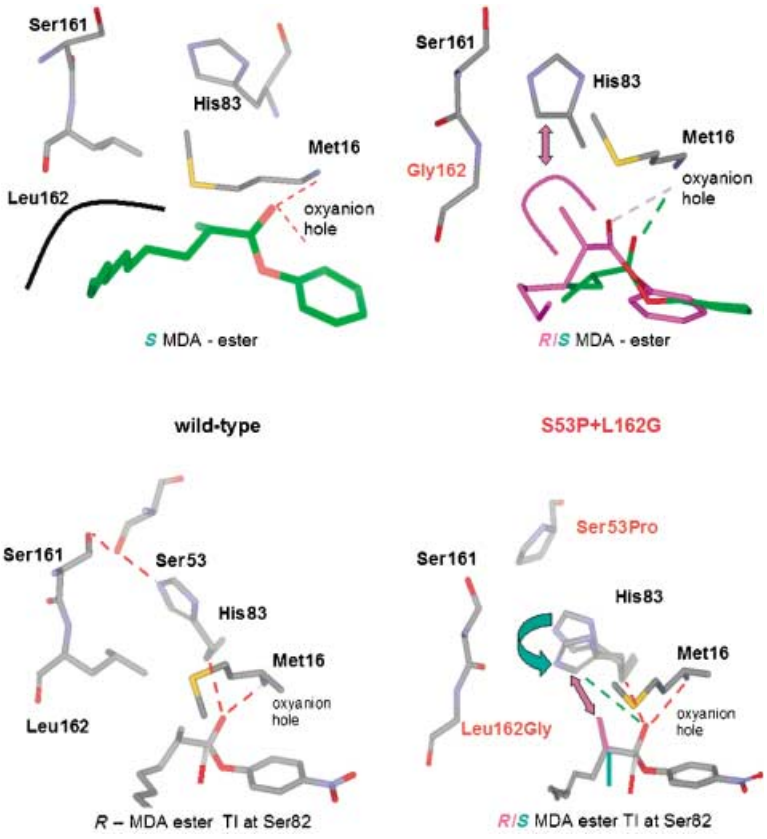

Figure 5. *Comparison between the wild-type (left) and the double mutant S53P + L162G (right). In the wild-type, His83 is held in place by a H bond network containing Ser161 and Ser53, and a direct van der Waals contact to Leu162 blocks any movement of His83 toward the active site. In the double mutant S53P + L162G this H bond network is disrupted and the side chain of residue 162 is removed, thus liberating His83 and allowing it to become a member of the active site residues in the binding pocket (see text).*

to provide additional stabilization, such as in the double mutant S53P + L162G through His83: in the wild-type structures (both X-ray and CHARMM MD) His83 is held in place by a hydrogen bond network containing Ser161 and Ser53; after disruption of this network by the replacement of S53P and the removal of the steric hindrance by the exchange L162G, His83 can move toward the active site and, in the case of the *S* enantiomer, establish a new hydrogen bond (see above). It is obvious that the two mutations S53P + L162G play a synergistic role in stabilizing the *S* enantiomer of the tetrahedral intermediate relative to the *R* enantiomer and thereby enhance enantioselectivity in a cooperative manner. For the sake of completeness, we note that these two mutations do not significantly alter the overall backbone geometry (monitored in the MD trajectories for both enantiomers through the relevant dihedral angles; data not shown).

The analogous formation of an extra hydrogen bond involving His83 is also observed in the MD simulations for the *S* enantiomers of the triple mutant S53P + S155M + L162G and the best mutant 1H8 (which incorporates the mutations S53P + L162G). This is compatible with the experimental finding[4] that residue 162 is a "hot spot" during directed evolution and that there are several other successful enantioselective mutants containing L162G. The current MD simulations explain the importance of this exchange for enantioselectivity in terms of the possible generation of a new binding pocket.

Experimentally, even the single mutant L162G is fairly enantioselective ($E = 34$).[4c] This effect is not captured by the current MD approach, since His83 remains hydrogen-bonded to Ser53 during the 1 ns simulations even for the *S* enantiomer. We have, however, confirmed that His83 will also stabilize the *S* enantiomer of the tetrahedral intermediate in L162G through an additional hydrogen bond if it is placed manually at a suitable position. No such position is reached during our limited simulation time, since movement of His83 is an activated process in L162G.

Energies

We have evaluated some energetic descriptors of enantioselectivity. Consistently with the qualitative arguments in the preceding section and with previous modeling studies in the literature[16] we have focused on the nonbonded interaction energies from the CHARMM MD simulations. Table 4 and Table 5 summarize the corresponding average values and their standard deviations for all investigated variants of the Michaelis – Menten complex and of the tetrahedral intermediate, respectively.

The total nonbonded interaction energies (van der Waals and electrostatic terms) are fairly uniform for the Michaelis – Menten complexes, and the corresponding differences for the *R* and *S* enantiomers are small and unsystematic, especially when the underlying fluctuations are considered (Table 4). In the case of the mutant 1H8, the measured Michaelis – Menten constants (k_m) of the *R* and *S* substrate do not differ too much, so small energy differences are to be expected for this mutant.

The differences between the *R* and *S* enantiomers are somewhat larger for the tetrahedral intermediates (Table 5). A clear preference for the *S* enantiomers is seen for the best mutant 1H8 (in agreement with experiment), for the two triple mutants, and for the double mutant S53P + L162G, which is at least partly due to the electrostatic terms. The geometric

Table 4. *Energetic descriptors[a] in the (R)- and (S)-MDA ester complex for the wild-type enzyme and different mutants.[b]*

	wild-type	1H8	S53P S155M L162G	S53P S155F L162G	S53P L162G	S155F L162G	S53P	S155M	S155F	L162G
difference $\Delta_{S-R}\Delta E$ in										
total interaction energy	−3.9	−1.7	−7.8	−4.0	1.1	−1.8	2.0	−0.4	−2.9	−1.8
total interaction energy *S*	−41.2 ± 3	−40.6 ± 3	−46.5 ± 3	−41.7 ± 3	−42.5 ± 3	−41.8 ± 2	−40.0 ± 2	−43.9 ± 2	−43.1 ± 3	−45.3 ± 2
total interaction energy *R*	−37.3 ± 4	−38.9 ± 3	−38.7 ± 2	−37.7 ± 2	−43.6 ± 4	−40.0 ± 3	−42.0 ± 3	−43.5 ± 2	40.3 ± 2	−43.5 ± 2

[a] Total nonbonded interaction energies [kcal mol^{-1}] between the atoms of the MDA ester and all other protein atoms (van der Waals plus electrostatic interactions). [b] See footnote [b] in Table 1.

Table 5. *Energetic descriptors[a] in the (R)- and (S)-MDA ester TI for the wild-type enzyme and different mutants.[b]*

	wild-type	1H8	S53P S155M L162G	S53P S155F L162G	S53P L162G	S155F L162G	S53P	S155M	S155F	L162G
difference $\Delta_{S-R}\Delta E$ in										
total interaction energy	8.7	−12.2	−18.2	−11.4	−9.9	−5.6	−1.6	0.4	0.5	−2.2
total interaction energy *S*	−75.7 ± 4	−94.4 ± 5	−100.0 ± 4	−89.4 ± 6	−92.9 ± 5	−87.3 ± 7	−81.6 ± 4	−80.1 ± 7	−84.8 ± 6	−82.8 ± 4
total interaction energy *R*	−84.4 ± 4	−82.2 ± 6	−81.8 ± 4	−78.0 ± 6	−83.0 ± 4	−82.9 ± 7	−80.0 ± 5	−80.5 ± 5	−85.3 ± 7	−80.6 ± 4
difference $\Delta_{S-R}\Delta E$ in										
electrostatic interaction	1.1	−7.0	−12.7	−5.5	−4.6	3.3	−1.0	−4.7	3.8	−1.4
electrostatic interaction *S*	−75.7 ± 4	−84.0 ± 4	−87.9 ± 4	−80.0 ± 4	−82.9 ± 5	−75.3 ± 4	−75.0 ± 4	−81.7 ± 3	−76.5 ± 4	−75.1 ± 4
electrostatic interaction *R*	−76.6 ± 4	−77.0 ± 4	−75.2 ± 4	−74.5 ± 4	−78.3 ± 4	−78.6 ± 4	−74.0 ± 4	−77.0 ± 3	−80.3 ± 4	−73.7 ± 4

[a] Total nonbonded interaction energies [kcal mol^{-1}] between the atoms of the MDA ester TI (same atoms as in Table 4) and all other protein atoms, excluding the covalently bound serine Oγ atom. The electrostatic contributions [kcal mol^{-1}] are listed separately. [b] See footnote [b] in Table 1.

evaluations have shown (Table 3) that in most of these cases the *S* enantiomer has an additional hydrogen bond involving His83, which should be associated with extra electrostatic stabilization. In this sense, the energy partitioning in Table 5 is consistent with the structural evaluations.

Conclusion

Directed evolution of the lipase from *Pseudomonas aeruginosa* has led to the creation of a highly enantioselective mutant with six mutational changes. In order to explain the direction and extent of enantioselectivity, we propose a model that focuses mainly on two mutations (L162G and S53P), one near the active site and the other remote from the oxy-anion hole. The synergistic effect of these two mutations has two consequences. Firstly, a new binding pocket for α-chiral esters is created. Secondly, stereoselectivity in favor of the *S* enantiomer is due to a relay effect in which a histidine moves toward the oxy-anion and exerts stabilization by H bonding. This is not possible in the case of the *R* enantiomer for steric reasons. It is unlikely that the highly enantioselective mutant 1H8 would have been found by rational protein engineering based on site-specific mutagenesis. Moreover, the theoretical analysis presented here shows that important structural and mechanistic lessons can be learned from directed evolution.

The other four mutations found in the optimized lipase variant 1H8 are located outside the active site, near to or at the surface of the lipase (see Figure 2). Their possible role was studied in more detail only for Ser155. The influence of residue 155 seems to be counterproductive in this context, since the structural evaluation indicates that the moderately selective S155F variant found by directed evolution may act by a steric relay through L162. After the replacement L162G this is no longer possible, and therefore the introduction of S155F should not increase the enantiopreference in an additive or cooperative manner. In fact, it actually reduces stereoselectivity by partially occupying the newly created binding pocket from the top of the binding site. The experimental results[4e] for a mutant containing the double mutation 1A11 (S155F + L162G) indeed reveal a significantly decreased enantioselectivity of $E = 22$ relative to the experimentally determined single mutant 1A1 (L162G) with $E = 34$. Our simulations show no qualitative changes for the triple mutant S53P + S155M + L162G relative to the best mutant 1H8, which contains all six mutations, thus suggesting that the omitted set of distinct mutations containing D20N, T180I, and T234S (see Table 1) make no significant contribution to the enantioselectivity. These mutations are already present in the parental lipase mutants, which exhibit only minor enantioselectivity experimentally. We therefore conclude from the results of our simulations that these surface mutations, accumulated in the directed evolution process, are not significant for enantioselectivity. These mutations may contribute to the activity and stability of the stereoselective lipase variant under assay conditions, but this is currently uncertain because we did not simulate such parameters. It should be mentioned that the high-throughput assay used in screening for enantioselectivity also responds to activity.

In order to corroborate the conclusions of this study, further QM/MM investigations with the enzyme mutants are required. These should focus on the calculation of the full reaction path, including the transition states of both enantiomers. It should also be of interest to apply theory for understanding the reversal of enantioselectivity that we recently accomplished by directed evolution.[4d] Finally, the theoretical insights into lipase enantioselectivity presented here may be used as a guide in designing further experiments and help to improve rational enzyme engineering.

Computational Methods

Model building: The wild-type and mutant structures were constructed from the X-ray crystal structure of *Pseudomonas aeruginosa* lipase complexed with *R*c-(*R*p,*S*p)-1,2-dioctylcarbamoylglycero-3-*O*-octylphosphonate[10a] (PDB code 1EX9) obtained from the Protein Data Bank. The tetrahedral inhibitor covalently bound to Ser82 was excised and replaced by the (*R*,*S*)-1-methyldecanoic acid phenol ester (MDA ester) or the corresponding tetrahedral intermediate (MDA ester TI) bound to Ser82. Two binding modes (rotamers) were used as starting geometries for each enantiomer, as depicted in Scheme 5.

Preparation: The protonation state of the protein was assigned at pH 7 by use of Insight2000[19] and the protonation of the His residues was revised to achieve best donor–acceptor interactions. The residues His81 and His109 were changed from HSD to HSE. His238

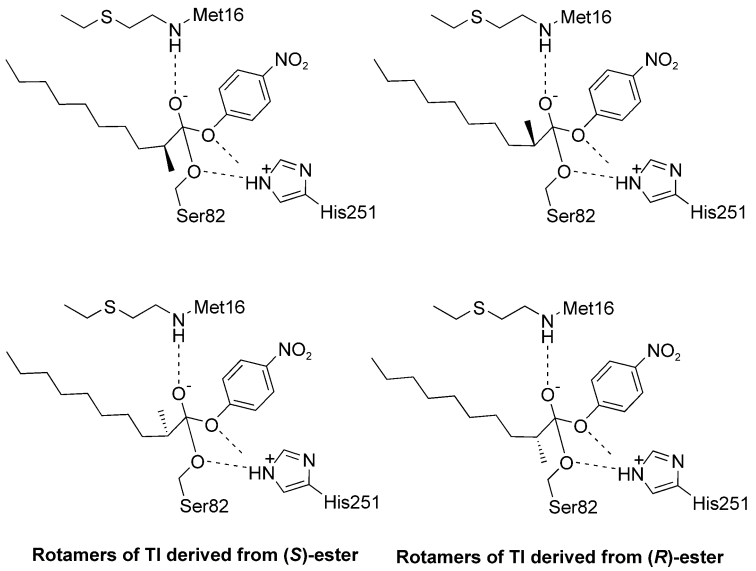

Scheme 5. *Models of (R)-/(S)-α-methyldecanoic acid* p*-nitrophenyl ester tetrahedral intermediates. Two stable rotamers of the α-MDA moiety in the acyl binding site of* P. aeruginosa *lipase are possible. The long acid chain always points into the acyl pocket toward the surface of the enzyme, whereas the methyl group at the stereocenter in the α-position to the reaction center can be oriented to the top or bottom of the binding pocket. In the rotamers for the slowly reacting* R *enantiomer shown on the right, either the methyl group (top) or the acid chain (bottom) is in an unfavorable gauche position toward the oxy-anion.*

was assumed to be a protonated HSP residue forming a salt bridge to Asp245. The catalytic His251 was assumed to be HSD forming a H bond to the charged Asp229 in the ester complex and to Ser82. In the TI the proton from Ser82Oγ was removed and Ser82Oγ is covalently bound to the tetrahedral hemiacetal carbon. His251 was set as charged HSP, donating a H bond to the Ser82Oγ and the MDA ester TI. To avoid electrostatic repulsion, Glu254 was protonated. In the X-ray crystal structure (1ex9)[10a] this residue exhibits a direct 2.65 Å contact from Oε2 toward Oδ2 of the negatively charged catalytic Asp229 in a typical H bond geometry, and Glu254 is therefore assumed to be a H-bond donor. The mutants were constructed with Insight2000 BIOPOLYMER by use of the automatic rotamer assignment and were energy-minimized by MOLOC or CHARMM 29b2 through a conjugate gradient algorithm using a stepwise decreasing harmonic constraint on all atoms.

Force-field parameters: The standard CHARMM potential function[18e] was used with the CHARMM22/27 parameter set.[18a–c] The latter contains no appropriate parameters for the negatively charged tetrahedral hemiacetal, so we derived CHARMM-type parameters for this group by established procedures.[18, 20] The parameters were calibrated against target data obtained mainly from ab initio Hartree–Fock and density functional calculations (optimized geometries, adiabatic rotational barriers, and intermolecular interaction energies).[21] By using the resulting parameter set it is possible to simulate the tetrahedral intermediates of various substrates in the active site of the lipase mutants under investigation. The MDA-*p*-nitrophenyl esters were modeled as phenyl esters.

MOLOC/MAB minimizations and MD simulations: The wild-type and the mutants were initially minimized. Thereafter, MD simulations of 1 ns were performed by use of the force-field MAB as implemented in MOLOC[17] (Version 10/02) with implicit solvation. No additional parameterization for the substrates was needed. We used a H-bond weight of 1.78 corresponding to the H-bond strength parameterized for the binding enthalpy rather than for the binding free energy.

CHARMM MD simulations: The enzyme/substrate complex was solvated with a preequilibrated 20 Å water droplet around the active site (substrate atom C9). The droplet boundary of 2.5 Å was constrained with a quartic force of 0.2 [24 kcal mol^{-1} Å^{-2}] by use of MMFP. All hydrogen atoms were held by SHAKE. Protein residues more than 20 Å away from the substrate stereocenter (substrate atom C1) in the active site were fixed. At first only the water shell and subsequently the solvated enzyme/substrate complex were energy-minimized, with the use of a distance constraint of 2.0 Å (1.8 Å) between the carbonyl oxygen (oxy-anion) and the backbone NH of Met 16 in the oxy-anion hole. This RESD constraint used a force constant of 50 kcal mol^{-1} Å^{-2} to preserve the enzyme/substrate interaction during the preparation phase. The system was heated from 100 K to 300 K with a 1 fs time step and 5 K temperature increase every 10 time steps. Thereafter it was allowed to relax at 300 K over 50000 time steps. The constrained force on the enzyme-substrate C=O:HN interaction was then decreased stepwise over additional MD cycles (5000 steps each) at 300 K until it vanished.

CHARMM production runs and evaluation: For production runs at 300 K a 2 fs time step was used over 500000 steps (1000 ps). The coordinates were saved every 1000 steps. All runs were performed twice with different initial velocities and with different starting geometries for both enantiomers. The first 300 ps were regarded as an equilibration phase to let the constructed mutants relax and the following 700 ps were analyzed. We statistically evaluated several geometric and energetic descriptors over the production phase within the CHARMM suite of programs and calculated the average values and standard deviations. Nonbonded interaction energies between the substrate ester or the substrate TI and the full protein environment were calculated from the standard CHARMM potential function[18] (van der Waals and electrostatic terms only). In the case of the TI we omitted the covalently bound Ser82Oγ to obtain reasonable van der Waals interaction energies. The electrostatic interaction energies were computed from the usual point-charge expression.[18]

Acknowledgements

Support by the Fonds der Chemischen Industrie is gratefully acknowledged.

Keywords: directed evolution · enantioselectivity · enzyme catalysis · molecular dynamics · molecular modeling

[1] a) *Directed Molecular Evolution of Proteins* (Eds.: S. Brakmann, K. Johnsson), Wiley-VCH, Weinheim, **2002**; b) *Directed Evolution Library Creation: Methods and Protocols* (Eds.: F. H. Arnold, G. Georgiou), Humana Press, Totowa, NJ, **2003**; c) *Directed Enzyme Evolution: Screening and Selection Methods* (Eds.: F. H. Arnold, G. Georgiou), Humana Press, Totowa, NJ, **2003**; d) *Enzyme Functionality* (Ed.: A. Svendsen), Marcel Dekker, New York, **2003**.

[2] K. A. Powell, S. W. Ramer, S. B. del Cardayré, W. P. C. Stemmer, M. B. Tobin, P. F. Longchamp, G. W. Huisman, *Angew. Chem.* **2001**, *113*, 4068–4080; *Angew. Chem. Int. Ed.* **2001**, *40*, 3948–3959.

[3] a) D. W. Leung, E. Chen, D. V. Goeddel, *Technique (Philadelphia)* **1989**, *1*, 11–15. See also: b) K. A. Eckert, T. A. Kunkel, *PCR Methods Appl.* **1991**, *1*, 17–24; c) R. C. Cadwell, G. F. Joyce, *PCR Methods Appl.* **1994**, *3*, S136–S140; d) M. T. Reetz, K.-E. Jaeger, *Top. Curr. Chem.* **1999**, *200*, 31–57.

[4] a) M. T. Reetz, A. Zonta, K. Schimossek, K. Liebeton, K.-E. Jaeger, *Angew. Chem.* **1997**, *109*, 2961–2963; *Angew. Chem. Int. Ed. Engl.* **1997**, *36*, 2830–2832; b) K. Liebeton, A. Zonta, K. Schimossek, M. Nardini, D. Lang, B. W. Dijkstra, M. T. Reetz, K.-E. Jaeger, *Chem. Biol.* **2000**, *7*, 709–718; c) M. T. Reetz, S. Wilensek, D. Zha, K.-E. Jaeger, *Angew. Chem.* **2001**, *113*, 3701–3703; *Angew. Chem. Int. Ed.* **2001**, *40*, 3589–3591; d) D. Zha, S. Wilensek, M. Hermes, K.-E. Jaeger, M. T. Reetz, *Chem. Commun.* **2001**, 2664–2665; e) S. Wilensek, Dissertation, Ruhr-Universität Bochum (Germany), **2001**.

[5] a) M. T. Reetz, *Pure Appl. Chem.* **2000**, *72*, 1615–1622; b) M. T. Reetz, K.-E. Jaeger, *Chem. Eur. J.* **2000**, *6*, 407–412; c) "Directed Evolution as a Means to Create Enantioselective Enzymes for Use in Organic Chemistry" M. T. Reetz, K.-E. Jaeger in *Directed Molecular Evolution of Proteins* (Eds.: S. Brakmann, K. Johnsson), Wiley-VCH, Weinheim, **2002**, pp. 245–279; d) M. T. Reetz, *Tetrahedron* **2002**, *58*, 6595–6602.

[6] a) M. T. Reetz, *Angew. Chem.* **2001**, *113*, 292–320; *Angew. Chem. Int. Ed.* **2001**, *40*, 284–310; b) M. T. Reetz, *Angew. Chem.* **2002**, *114*, 1391–1394; *Angew. Chem. Int. Ed.* **2002**, *41*, 1335–1338; c) M. T. Reetz, A. Eipper, P. Tielmann, R. Mynott, *Adv. Synth. Catal.* **2002**, *344*, 1008–1016.

[7] a) A. R. Fersht, *Biochemistry* **1987**, *26*, 8031–8037; b) P. N. Bryan, *Biotechnol. Adv.* **1987**, *5*, 221–234; c) J. A. Gerlt, *Chem. Rev.* **1987**, *87*, 1079–1105; d) J. R. Knowles, *Science* **1987**, *236*, 1252–1258; e) S. J. Benkovic, C. A. Fierke, A. M. Naylor, *Science* **1988**, *239*, 1105–1110; f) J. A. Wells, D. A. Estell, *Trends Biochem. Sci.* **1988**, *13*, 291–297; g) Y. Hirose, K. Kariya, Y. Nakanishi, Y. Kurono, K. Achiwa, *Tetrahedron Lett.* **1995**, *36*, 1063–1066; h) Z. Shao, F. H. Arnold, *Curr. Opin. Struct. Biol.* **1996**, *6*, 513–518; i) D. Rotticci, J. C. Rotticci-Mulder, S. Denman, T. Norin, K. Hult, *ChemBioChem* **2001**, *2*, 766–770; j) J. Pleiss in *Enzyme Functionality* (Ed.: A. Svendsen), Marcel Dekker, New York, **2003**, pp. 59–77.

[8] H. Zhao, F. H. Arnold, *Protein Eng.* **1999**, *12*, 47–53.

[9] See for example: a) A. Iffland, P. Tafelmeyer, C. Saudan, K. Johnsson, *Biochemistry.* **2000**, *39*, 10790–10798; b) M. Kumar, K. K. Kannan, M. V. Hosur, N. S. Bhavesh, A. Chatterjee, R. Mittal, R. V. Hosur, *Biochem. Biophys. Res. Commun.* **2002**, *294*, 395–401; c) P. K. Agarwal, S. R. Billeter, P. T. Rajagopalan, S. J. Benkovic, S. Hammes-Schiffer, *Proc. Natl. Acad. Sci. USA*

2002, *99*, 2794 – 2799; d) F. H. Arnold, P. L. Wintrode, K. Miyazaki, A. Gershenson, *Trends Biochem. Sci.* **2001**, *26*, 100 – 106; e) G. P. Horsman, A. M. F. Liu, E. Henke, U. T. Bornscheuer, R. J. Kazlauskas, *Chem. Eur. J.* **2003**, *9*, 1933 – 1939.

[10] a) M. Nardini, D. A. Lang, K. Liebeton, K. E. Jaeger, B. W. Dijkstra, *J. Biol. Chem.* **2000**, *275*, 31 219 – 31 225; b) G. van Pouderoyen, T. Eggert, K.-E. Jaeger, B. W. Dijkstra, *J. Mol. Biol.* **2001**, *309*, 215 – 226.

[11] a) A. Fersht, *Structure and Mechanism in Protein Sciences: A Guide to Enzyme Catalysis and Protein Folding*, Freeman, New York, **1998**; b) R. B. Silverman, *The Organic Chemistry of Enzyme-Catalyzed Reactions*, Academic Press, London, **2000**.

[12] a) E. Henke, U. T. Bornscheuer, *Biol. Chem.* **1999**, *380*, 1029 – 1033; b) O. May, P. T. Nguyen, F. H. Arnold, *Nat. Biotechnol.* **2000**, *18*, 317 – 320; c) S. Fong, T. D. Machajewski, C. C. Mak, C. H. Wong, *Chem. Biol.* **2000**, *7*, 873 – 883.

[13] a) K.-E. Jaeger, B. W. Dijkstra, M. T. Reetz, *Annu. Rev. Microbiol.* **1999**, *53*, 315 – 351; b) R. D. Schmid, R. Verger, *Angew. Chem.* **1998**, *110*, 1694 – 1720; *Angew. Chem. Int. Ed.* **1998**, *37*, 1608 – 1633; c) M. T. Reetz, *Curr. Opin. Chem. Biol.* **2002**, *6*, 145 – 150.

[14] a) A. D. Becke, *Phys. Rev. A* **1988**, *38*, 3098 – 3100; b) C. Lee, W. Yang, R. G. Parr, *Phys. Rev. B* **1988**, *37*, 785 – 789; c) Gaussian98, Revision A.7, M. J. Frisch, G. W. Trucks, H. B. Schlegel, G. E. Scuseria, M. A. Robb, J. R. Cheeseman, V. G. Zakrzewski, J. A. Montgomery, Jr., R. E. Stratmann, J. C. Burant, S. Dapprich, J. M. Millam, A. D. Daniels, K. N. Kudin, M. C. Strain, O. Farkas, J. Tomasi, V. Barone, M. Cossi, R. Cammi, B. Mennucci, C. Pomelli, C. Adamo, S. Clifford, J. Ochterski, G. A. Petersson, P. Y. Ayala, Q. Cui, K. Morokuma, D. K. Malick, A. D. Rabuck, K. Raghavachari, J. B. Foresman, J. Cioslowski, J. V. Ortiz, A. G. Baboul, B. B. Stefanov, G. Liu, A. Liashenko, P. Piskorz, I. Komaromi, R. Gomperts, R. L. Martin, D. J. Fox, T. Keith, M. A. Al-Laham, C. Y. Peng, A. Nanayakkara, C. Gonzalez, M. Challacombe, W. Gill, P. M. B. Johnson, W. Chen, M. W. Wong, J. L. Andres, C. Gonzalez, M. Head-Gordon, E. S. Replogle, J. A. Pople, Gaussian, Inc., Pittsburgh, PA, **1998**.

[15] a) T. Ema, J. Kobashi, S. Maeno, T. Sakai, M. Utaka, *Bull. Chem. Soc. Jpn.* **1998**, *71*, 443 – 453; b) C. H. Hu, T. Brinck, K. Hult, *Int. J. Quantum Chem.* **1998**, *69*, 89 – 103.

[16] a) J. Zuegg, H. Hönig, J. D. Schrag, M. Cygler, *J. Mol. Catal. B: Enzym.* **1997**, *3*, 83 – 98; b) H. Scheib, J. Pleiss, P. Stadler, A. Kovac, A. P. Potthoff, L. Haalck, F. Spener, F. Paltauf, R. D. Schmid, *Protein Eng.* **1998**, *11*, 675 – 682; c) F. Hæffner, T. Norin, K. Hult, *Biophys. J.* **1998**, *74*, 1251 – 1262; d) T. Schulz, J. Pleiss, R. D. Schmid, *Protein Sci.* **2000**, *9*, 1053 – 1062; e) A. Tafi, A. van Almsick, F. Corelli, M. Crusco, K. E. Laumen, M. P. Schneider, M. Botta, *J. Org. Chem.* **2000**, *65*, 3659 – 3665; f) M. Luić, S. Tomić, I. Leščić, E. Ljubović, D. Šepać, V. Šunjić, L. J. Vitale, W. Saenger, B. Kojić-Prodić, *Eur. J. Biochem.* **2001**, *268*, 3964 – 3973; f) S. Raza, L. Fransson, K. Hult, *Protein Sci.* **2001**, *1*, 329 – 338; g) S. Tomić, V. Dobovičnik, V. Šunjić, B. Kojić-Prodić, *Croat. Chem. Acta* **2001**, *74*, 343 – 357; h) S. Tomić, B. Kojić-Prodić, *J. Mol. Graph. Model.* **2002**, *21*, 241 – 252; i) M. Bocola, M. T. Stubbs, C. Sotriffer, B. Hauer, T. Friedrich, K. Dittrich, G. Klebe, *Protein Eng.* **2003**, *16*, 319 – 322; j) E. Henke, U. T. Bornscheuer, R. D. Schmid, J. Pleiss, *ChemBioChem* **2003**, *4*, 485 – 493. k) R. Kazlauskas, *Science* **2001**, *293*, 2277 – 2279.

[17] a) P. R. Gerber, *J. Comput.-Aided Mol. Des.* **1998**, *12*, 37 – 51; b) P. R. Gerber, K. Müller, *J. Comput.-Aided Mol. Des.* **1995**, *9*, 251 – 268.

[18] a) A. D. MacKerell, D. Bashford, M. Bellott, R. L. Dunbrack, J. D. Evanseck, M. J. Field, S. Fischer, J. Gao, H. Guo, S. Ha, D. Joseph-McCarthy, L. Kuchnir, K. Kuczera, F. T. K. Lau, C. Mattos, S. Michnick, T. Ngo, D. T. Nguyen, B. Prodhom, W. E. Reiher, B. Roux, M. Schlenkrich, J. C. Smith, R. Stote, J. Straub, M. Watanabe, J. Wiorkiewicz-Kuczera, D. Yin, M. Karplus, *J. Phys. Chem. B* **1998**, *102*, 3586 – 3616; b) J. J. Pavelites, J. L. Gao, P. A. Bash, A. D. MacKerell, *J. Comput. Chem.* **1997**, *18*, 221 – 239; c) N. Foloppe, A. D. MacKerell, *J. Comput. Chem.* **2000**, *21*, 86 – 104; d) A. D. J. MacKerell, D. Bashford, M. Bellott, Jr., R. L. Dunbrack, M. J. Field, S. Fischer, J. Gao, H. Guo, S. Ha, D. Joseph, L. Kuchnir, K. Kuczera, F. T. K. Lau, C. Mattos, S. Michnick, T. Ngo, D. T. Nguyen, B. Prodhom, B. Roux, M. Schlenkrich, J. C. Smith, R. Stote, J. Straub, J. Wiorkiewicz-Kuczera, M. Karplus, *FASEB J.* **1992**, *6A*, 143; e) B. R. Brooks, R. E. Bruccoleri, B. D. Olafson, D. J. States, S. Swaminathan, M. Karplus, *J. Comput. Chem.* **1983**, *4*, 187 – 217.

[19] INSIGHTII, Accelrys Inc., San Diego, USA, **2000**.

[20] N. Reuter, H. Lin, W. Thiel, *J. Phys. Chem. B* **2002**, *106*, 6310 – 6321.

[21] N. Otte, M. Bocola, W. Thiel, unpublished results. The parameters are available from the authors on request.

Received: July 31, 2003 [F 731]

